pic and acac

Electron-donating substituents are used to fine-tune the redox properties of sky-blue cyclometallated iridium complexes and improve electroluminescence performance.

Tuning the Oxidation Potential of 2-Phenylpyridine-based Iridium Complexes to Improve the Performance of Bluish and White OLEDs

Yafei Wang[†‡Δ], Ning Sun[‖Δ], Basile F. E. Curchod[&], Louise Male[†], Dongge Ma[‖*], Jiang Fan[‡], Yu Liu[‡], Weiguo Zhu[‡*], Etienne Baranoff[†*]

† *School of Chemistry, University of Birmingham, Birmingham B15 2TT, UK*

‡ *Department of Chemistry, Key Lab of Environment-Friendly Chemistry and Application in the Ministry of Education, Xiangtan University, Xiangtan 411105, P. R. China.*

‖ *State Key Laboratory of Polymer Physics and Chemistry, Changchun Institute of Applied Chemistry, Chinese Academy of Sciences, Changchun 130022, P. R. China*

& *Department of Chemistry, Stanford University, Stanford, CA 94305-5080, USA*

Δ *The authors contributed equally to this work*

Corresponding authors

DG Ma: mdg1014@ciac.jl.cn

WG Zhu: zhuwg18@126.com

E Baranoff: e.baranoff@bham.ac.uk

Abstract

The use of electron-withdrawing substituents on the orthometallated phenyl is a common strategy to blue shift the emission of cyclometalated iridium complexes by stabilizing the highest occupied molecular orbital (HOMO), that is increasing the oxidation potential of the complex. However, for application in blue organic light-emitting diodes (OLEDs), this approach imposes host materials with deep HOMO, which negatively impacts the injection of charges, hence the performance of the devices. In this context, we report new iridium complexes with an electron-donating substituent on the cyclometalated ligand to blue shift the emission while keeping relatively low oxidation potential. As a result, bluish-green OLEDs based on host materials with shallow HOMO (TCTA = 4,4′,4″-tri(N-carbazolyl)-triphenylamine) display higher performance than device using FIrpic in the same architecture. The improvements are primarily attributed to the lower turn-on voltage (2.8 to 3 V) compared to FIrpic-device (3.6 V). White OLED was then prepared with maximum brightness of 20,226 cd m^{-2} and current efficiency of 20.4 cd A^{-2} (at 100 cd m^{-2}). Interestingly, very small efficiency roll-off of about 1% at 1000 cd m^{-2} and high color stability was achieved. At luminance level of 5,000 cd m^{-2} the roll-off efficiency is still below 20%. The introduction of electron-donating substituents on a 2-phenylpyridine scaffold to obtain blue emitters with low oxidation potentials provides an alternative to strategies based on replacing the pyridine with imidazole, carbene, and pyrazole.

Introduction

Phosphorescent organic light-emitting diodes (PhOLEDs) are very attractive for highly efficient lighting applications due to the ability of phosphorescent materials to utilize both the singlet and triplet excitons leading to devices with possibly 100% internal quantum yield.[1-3] Although significant progresses are continuously being made,[4-6] several challenges still remain for blue and white PhOLEDs application as commercial products for lighting, for instance in terms of device stability, fabrication costs and for the severe efficiency roll-off at high luminance at brightness >1000 cd m^{-2}.[7]

The ligand 2-phenylpyridine (ppy) is the most used core ligand for the design of iridium-based phosphorescent emitter: generally it is straightforward to synthesize and to chemically modify, and the resulting complexes have mostly good chemical, photochemical, and electrochemical stability.[8, 9] Starting from the standard green emitter Ir(ppy)$_3$, the design of iridium-based blue phosphorescent emitters has relied mainly on two strategies. First, introduction of electron-withdrawing substituents on the orthometallated phenyl ring leads to stabilization of the highest occupied molecular orbital (HOMO) much more than the lowest unoccupied molecular orbital (LUMO). The increased HOMO-LUMO energy gap translates into a blue shift of the emission.[10, 11] This approach lead in particular to the widely used sky-blue emitter FIrpic (iridium(III)bis[(4,6-difluorophenyl)-pyridinato-N,C′]picolinate).[12, 13] Further blue shift of the emission is achieved simply by grafting an additional electron-withdrawing group (*e.g.* trifluoromethyl,[11] perfluorocarbonyl,[14, 15] ester,[15] cyano,[16] nitrogen[17]) between the two fluorine atoms. However, a challenge with that approach is the need for host materials with deep HOMO, in which case injection of charges can become difficult. For example, *p*-bis(triphenylsilyly)benzene (UGH2) (E^{IP}: 7.2 eV),[18] 6-bis(3-(carbazol-9-yl)phenyl)pyridine (26DCzPPy) (E^{IP}: 6.05 eV) and 3,5-bis(3-(carbazol-9-yl)phenyl)pyridine (35DCzPPy) (E^{IP}: 6.18 eV)[19] have been used as the host matrix for blue phosphorescent OLEDs.

The second common strategy to blue shift the emission is to replace the pyridine moiety of ppy with *N*-coordinating imidazole,[20, 21] *N*-heterocyclic carbene,[22, 23] and pyrazole.[24, 25] This increases the triplet energy of the cyclometalated ligand mainly by destabilizing the LUMO. The low oxidation potential of these complexes compared to ppy-based complexes with electron withdrawing substituents allows for host materials with shallow HOMO and efficient blue PhOLEDs have been demonstrated.[20, 23] However each design has intrinsic limitations: imidazoles easily degrade in the presence of oxygen,[26, 27] carbene-based complexes have long excited state lifetime, which impact on device performance at high luminance,[23] and pyrazole-based complexes are usually poorly emissive.[28]

Based on the aforementioned observations it is attractive to design a blue emitter based on the ppy scaffold and with shallow HOMO. Herein we report such a new emitting cyclometalated iridium complex and demonstrate that when combined with a commonly used host without deep HOMO (here TCTA = 4,4′,4″-tri(*N*-carbazolyl)-triphenylamine), improved efficiencies are obtained compared to the standard FIrpic emitter. Our design is based on 2-phenylpyridine grafted with a combination of an electron-donating ethyloxy group with two fluorine substituents on the phenyl of the ppy ligand. We have previously demonstrated that electron-donating substituents on the orthometalated phenyl ring can replace electron-withdrawing substituents to obtain blue emitting complexes;[29] their primary effect is to destabilize the energy level of the LUMO, which provides a strategy to tune the oxidation potentials independently of the energy of emission.

Two complexes with picolinate (**YF1**) and acetylacetonate (**YF2**) ancillary ligands have been synthesized and fully characterized by NMR, mass spectra and single crystal X-ray diffraction. The two complexes yield intense bluish-green emission, respectively. As anticipated the calculated HOMO energy levels are −5.5 eV for the pic complex and −5.3 eV for the acac complex, compared to −5.9 for FIrpic and −5.7 for the host TCTA. The monochromatic OLEDs employing **YF1/YF2** as the emitter exhibit luminescent efficiency of 19.6 cd A^{-1} and 26.0 cd A^{-1} at 100 cd m^{-2}, respectively. The devices have improved external quantum efficiency at 100 cd m^{-2}

(EQE, η_{ext} = 7.5 and 8.1%) compared to FIrpic (η_{ext} = 4.4%) while keeping reasonable efficiency roll-off ≤ 30% at luminance level of 5000 cd m^{-2} and high color stability. The improved performances are attributed to the fine tuning of the oxidation potential of the complexes, which leads to a significant decrease of the turn-on voltage of **YF1**/**YF2**–based devices (2.8 and 3 V, respectively) compared to FIrpic-based device (3.6 V). Finally, low efficiency roll-off and color stable white OLEDs based on **YF1** show luminance of 20226 cd m^{-2} at 11 V and current efficiency of 20.4 cd A^{-1} at 100 cd m^{-2}. Interestingly, very small efficiency roll-off of about 1% at 1000 cd m^{-2} and high color stability was achieved. Attractively, at luminance level of 5000 cd m^{-2} the roll-off efficiency is still better than 20%.

Experimental

General information

4-ethoxy-2,3-difluorophenylboronic acid was purchased from Shijiazhuang Sdyano Fine Chemical Co., Ltd. All other reagents were purchased from Aldrich and VWR and used as received. All reactions and manipulations were carried out under Ar atmosphere with the use of standard inert atmosphere techniques. ^{1}H NMR spectra were measured in CDCl$_3$ solution on a Bruker DPX (300 MHz and 400 MHz) NMR spectrometer with tetramethylsilane (TMS) as the internal standard. Mass spectra (MS) were recorded on a Bruker Autoflex TOF/TOF (MALDI-TOF) instrument using dithranol as a matrix. UV-vis absorption spectroscopy was measured by Shimadzu UV-265 spectrometer at room temperature. Fluorescence spectra were recorded on RF-5301 PC (Perkin Elmer) at room temperature in dichloromethane. Solutions of FIrpic in CH$_2$Cl$_2$ (Φ = 0.62)[30] were used as a reference. The equation $\Phi_s = \Phi_r(\eta_s^2 A_r I_s / \eta_r^2 A_s I_r)$ was used to calculate the quantum yields.[31] Time-resolved fluorescence lifetime measurements were carried out by using a Hamamatsu Quantaurus-Tau C11567-01 time-correlated single photon counting system. The quality of the fit has been judged by the fitting parameters such as χ^2 (<1.2) as well as the visual inspection of the residuals. Cyclic voltammetry (CV) was performed with a

three electrode electrochemical cell in a 0.1 M tetra(n-butyl)-ammonium hexafluorophosphate (TBAPF$_6$) solution in CH$_2$Cl$_2$ with scan rate 100 mV s^{-1} at room temperature under argon. A platinum disk, platinum wire and Ag/AgCl were used as working electrode, counter electrode and reference electrode, respectively. Ferrocene was added as an internal reference.

OLEDs preparation

The configuration of devices I and II is ITO/MoO$_3$ (8 nm)/N,N'-Bis-(1-naphthalenyl)-N,N'-bis-phenyl-(1,1'-biphenyl)-4,4'-diamine (NPB; 50 nm)/ TCTA (5 nm)/TCTA:8wt% **YF1** or **YF2** (10 nm)/2,2',2"-(1,3,5-Benzinetriyl)-tris(1-phenyl-1-H-benzimidazole) (TPBi; 30 nm)/LiF (1 nm)/Al. The configuration of devices III is ITO/MoO$_3$ (8 nm)/NPB (50 nm)/TCTA (5 nm)/TCTA:6wt% Bis(2-benzo[b]thiophen-2-ylpyridine)(acetylacetonate)iridium(III) [Ir(bt)$_2$(acac)] (6 nm)/TCTA: 8wt% **YF1** (3 nm)/TPBi (30 nm)/LiF(1 nm)/Al. NPB is used as the hole transporting layer; TPBi is used as the electron transporting layer (ETL). Additional details of the fabrication and testing procedures of OLEDs can be found in previous report.[32]
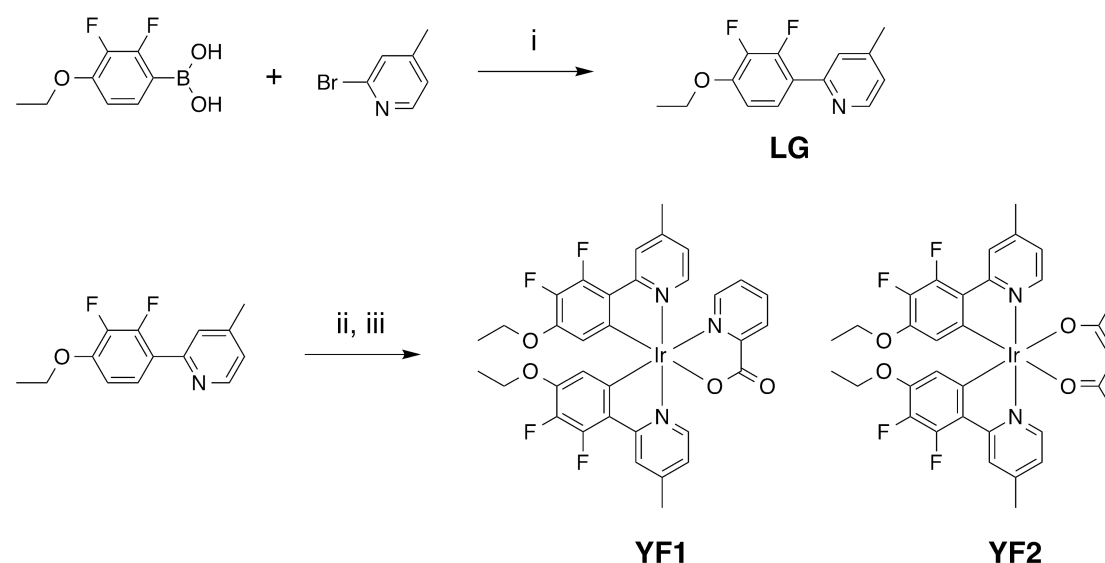
Scheme 1. Synthetic route for iridium complexes: i) 2M K$_2$CO$_3$, Pd(PPh$_3$)$_4$, toluene, ethanol, 85 ^{o}C, overnight. Yield: 81%; ii) LG, IrCl$_3$•3H$_2$O, 2-ethoxyethanol/H$_2$O = 3:1, 100°C, 16h; iii) TBAOH, picolinic acid (or acetylacetone), CH$_2$Cl$_2$, 40°C, overnight. Yield: **YF1**: 58%, **YF2**: 52%.

Synthesis of 2-(4-ethoxy-2,3-difluorophenyl)-4-methylpyridine (LG)

A mixture of 4-ethoxy-2,3-difluorophenylboronic acid (2.4 g, 11.7 mmol), 2-bromo-4-methylpyridine (2.0 g, 11.7 mmol), Pd(PPh$_3$)$_4$ (0.25 mmol, 0.29 g), aqueous K$_2$CO$_3$ (2M, 15 mL), ethanol (15 mL) and toluene (45 mL) was stirred at 85 $^{\circ}$C overnight under Ar. After cooling to RT, the reaction mixture was poured into 100 mL of water and extracted with CH$_2$Cl$_2$. The organic layers were washed with water, dried over MgSO$_4$ and the volatiles removed under vacuum. The residue was purified by column chromatography on silica (hexane/CH$_2$Cl$_2$ = 3:1) to give pure **LG** as a white solid (2.36 g, 81%). ^{1}H NMR (CDCl$_3$, 300 MHz): δ 8.54 (d, J = 5.1 Hz, 1H), 7.71-7.63 (m, 1H), 7.56 (s, 1H), 7.07 (d, J = 5.0 Hz, 1H), 6.88-6.80 (m, 1H), 4.18 (q, J = 7.0 Hz, 2H), 2.41 (s, 3H), 1.48 (t, J = 7.0 Hz, 3H). ^{13}C NMR (CDCl$_3$, 100 MHz): δ 152.4, 150.9, 149.5, 148.5, 147.6, 142.7, 140.2, 124.8, 124.2, 123.3, 121.5, 109.4, 65.3, 21.2, 14.7. ^{19}F NMR (CDCl$_3$, 282 MHz): −141.4, −159.6. MS (MALDI-TOF) m/z (M•Na$^+$): calcd. for C$_{14}$H$_{13}$F$_2$NO•Na, 272.1; found, 272.5.

General procedures for Ir(LG)$_2$(pic) (YF1) and Ir(LG)$_2$(acac) (YF2)

A mixture of **LG** (1.0 g, 4.0 mmol) and IrCl$_3$•3H$_2$O (0.56 g, 1.6 mmol) in a mixture of 2-ethoxylethanol (15 mL) and water (5 mL) was heated to 100 $^{\circ}$C for 16 h. After cooling down to room temperature, the precipitate of chloro-bridged iridium dimer was collected by filtration and washed with water and hexane. The yellow solid was used to the next step without any further purification. A mixture of picolinic acid (or acetylacetone) (2.2 eq), TBAOH (2.2 eq) and CH$_2$Cl$_2$/MeOH (V/V = 7:3) was added into the solution of the dimer (1 eq) in CH$_2$Cl$_2$. The reaction mixture was stirred at 40 $^{\circ}$C overnight. After cooling down to room temperature, the volatiles are removed under vacuum and the residue was purified by silica gel chromatography (CH$_2$Cl$_2$) to get the target iridium complexes.

YF1: Yellow solid, yield: 58%. ^{1}H NMR (CDCl$_3$, 300 MHz): δ 8.54 (d, J = 6.0 Hz, 1H), 8.30 (d, J = 7.5 Hz, 1H), 8.0-7.88 (m, 3H), 7.77 (d, J = 5.1 Hz, 1H), 7.40 (t, J = 6.0 Hz, 1H), 7.22 (d, J = 6.0 Hz, 1H), 6.93 (d, J = 5.7 Hz, 1H), 6.72 (d, J = 5.7 Hz, 1H), 3.76-3.68 (m, 4H), 2.52 (s, 6H), 1.24 (t, J = 6.0 Hz, 6H). ^{13}C NMR (CDCl$_3$, 100

MHz): δ 172.8, 165.9, 164.6, 152.0, 149.6, 148.2, 147.2, 142.9, 141.3, 141.3, 137.9, 128.4, 124.7, 124.4, 123.2, 122.6, 111.6, 64.6, 21.5, 14.6. ^{19}F NMR (CDCl$_3$, 282 MHz): −141.3, −170.1. MS (MALDI-TOF) *m/z* (M•Na^{+}): calcd. for C$_{34}$H$_{28}$F$_4$IrN$_3$O$_4$•Na, 834.2; found, 834.4.

YF2: Yellow solid, yield: 52%. ^{1}H NMR (CDCl$_3$, 300 MHz): δ 8.24 (d, *J* = 6.0 Hz, 2H), 7.96 (s, 2H), 6.95 (dd, *J* = 6.0 Hz, 1.5 Hz, 2H), 5.47 (dd, *J* = 7.5 Hz, 1.5 Hz, 2H), 5.22 (s, 1H), 3.77-3.65 (m, 4H), 2.58 (s, 6H), 1.80 (s, 6H), 1.22 (t, *J* = 6.9 Hz, 6H). ^{13}C NMR (CDCl$_3$, 100 MHz): δ 184.7, 165.7, 149.1, 148.2, 147.4, 141.1, 137.7, 135.5, 125.0, 122.5, 121.8, 112.1, 100.6, 64.1, 28.8, 21.5, 14.6. ^{19}F NMR (CDCl$_3$, 282 MHz):−140.5, −168.9. MS (MALDI-TOF) *m/z* (M•Na^{+}): calcd. for C$_{32}$H$_{32}$F$_4$IrN$_2$O$_4$•Na, 811.2; found, 811.6.
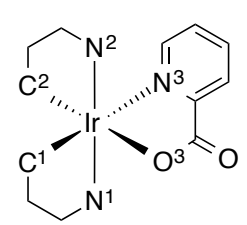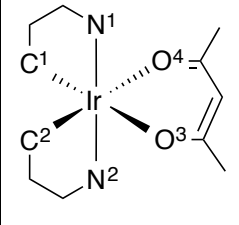
Results and Discussion

Synthesis and structure

The synthesis of the complexes is described in Scheme 1. The cyclometalated ligand (**LG**) was obtained in 81% yield via Suzuki coupling reaction directly from commercially available compounds. The chloro-bridged iridium dimer and the two target mononuclear iridium complexes were obtained according to reported procedures.[33] All compounds were characterized by ^{1}H NMR, ^{13}C NMR, ^{19}F NMR and TOF-MS. Single crystals of **YF1** and **YF2** suitable for X-ray diffraction were grown by slow diffusion of hexane into CH$_2$Cl$_2$ solutions of the complexes. The ORTEP diagrams of both iridium complexes and crystallographic parameters are given in ESI†. The iridium complexes possesses a distorted octahedral geometry with *trans*-N,N chelate configuration. The pendant ethyloxy unit is in the plane of the phenylpyridine. The different ancillary ligands have only a little influence on the overall structures. All the iridium-carbon (Ir-C) bond lengths are about 2.0 Å while the iridium-nitrogen (Ir-N) bond lengths are in the region of 2.03-2.14 Å. The iridium-oxygen (Ir-O) bond lengths are between 2.13-2.15 Å.

Table 1. Comparison between experimental and theoretical (DFT/ PBE0) ground state geometries.

Selected bond distances (Å) and angles (°)

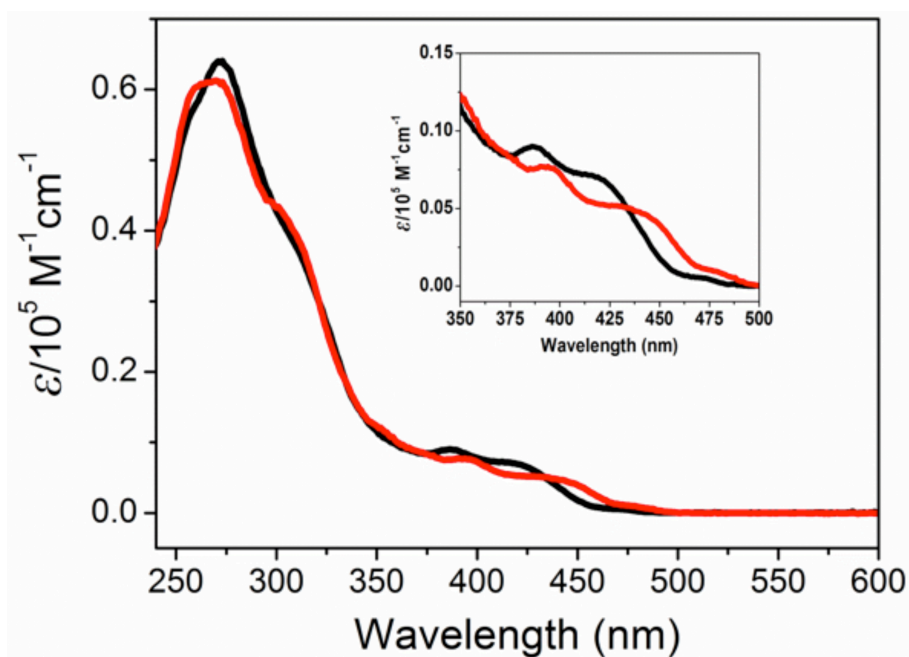|	X-ray	PBE0		X-ray	PBE0
Ir-N1	2.038(3)	2.050	**Ir-N1**	2.031(3)	2.038
Ir-C1	2.005(3)	2.007	**Ir-C1**	1.989(3)	1.991
Ir-N2	2.035(3)	2.036	**Ir-N2**	2.033(3)	2.038
Ir-C2	1.990(3)	1.996	**Ir-C2**	1.975(4)	1.991
Ir-O3	2.156(2)	2.156	**Ir-O4**	2.138(2)	2.159
Ir-N3	2.139(3)	2.152	**Ir-O3**	2.143(2)	2.159
N1-Ir-N2	173.77(11)	175.5	**N1-Ir-N2**	174.96(11)	177.2

Fig. 1 Absorption spectra of iridium complexes in CH_2Cl_2 at room temperature. Inset: the expanded absorption spectra in the range of 350 nm-500 nm. **YF1**: black line; **YF2**: red line.

Photophysical Properties

The electronic absorption spectra of **YF1** and **YF2** were measured in CH_2Cl_2 at room temperature (10^{-5} M, Fig. 1) and photophysical data are summarized in Table 2. Both iridium complexes exhibit intense absorption bands located at 250-325 nm with molar absorptivities (ε) on the order of $10^4 \, M^{-1} \, cm^{-1}$, which are attributed to the $^1\pi$-π^* transitions of cyclometalated ligands (LC).[34] The absorption bands from 350 nm to 450 nm with ε between 5×10^3 and $9 \times 10^3 \, M^{-1} \, cm^{-1}$ are assigned to metal-to-ligand charge transfer (MLCT) transitions.[35] Weak absorption bands around 470 nm with extinction coefficients ~$100 \, M^{-1} \, cm^{-1}$ originate from direct singlet to triplet ^{3}MLCT transitions (Fig. 1 inset).[36] The assignments of the transitions are further supported by theoretical calculations (see below). Compared to **YF1**, **YF2** exhibits a red-shifted absorption spectrum between 350-500 nm because of the weaker ligand-field of acetylacetonate compared to picolinate.
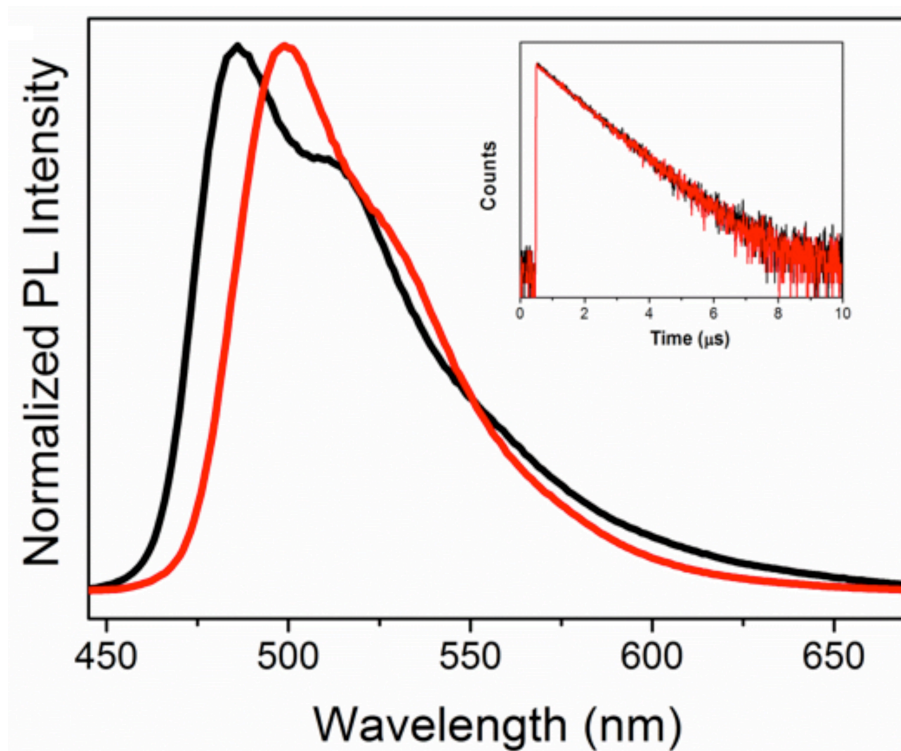

Fig. 2 Normalized PL spectra of iridium complexes in CH_2Cl_2 at room temperature. The inset shows the luminescence decay behavior at room temperature. **YF1**: black line; **YF2**: red line.

Table 2. Photophysical data of **YF1** and **YF2**

	Absorption/nm ($\varepsilon/10^4\,M^{-1}\,cm^{-1}$)	Emission /nm	$\Phi^{\,c}$	$\tau^{\,d}$ /μs	$k_r^{\,e}$ /$10^5\,s^{-1}$	$k_{nr}^{\,f}$ /$10^5\,s^{-1}$	$E_{ox}^{\,g}$ /V	$E_{HOMO}^{\,h}$ /eV	$E_{LUMO}^{\,h}$ /eV
YF1	272 (6.4), 308 (4.1), 388 (0.9), 422 (0.7), 474 (0.05)	485, 512 ^{a} 492, 527 ^{b}	0.52	1.37	3.79	3.51	0.77	−5.5	−2.8
YF2	270 (6.1), 301 (4.4), 395 (0.8), 444 (0.5), 483 (0.09)	499, 525 ^{a} 514 ^{b}	0.61	1.40	4.36	2.78	0.60	−5.3	−2.7

^{a} the emission were measured in CH_2Cl_2; ^{b} the emission were measured in neat film; ^{c}Measured in degassed DMF solution at room temperature using FIrpic ($\Phi = 0.62$) as reference; ^{d} Lifetime was evaluated in oxygen-free DMF; ^{e} Radiative decay rate $K_r = \Phi_{PL}/\tau$; ^{f} Nonradiative decay rate $k_{nr} = \tau^{-1} - k_r$; ^{g} $E_{ox} = \frac{1}{2}(I_{pc} + I_{pa})$; ^{h} E_{00} calculated from the edge of emission spectra; $E_{HOMO} = -(1.2 \times Eox + 4.6)$ eV and $E_{LUMO} = (E_{HOMO} + E_{00})$ eV..

The photoluminescent spectra (PL) of iridium complexes in CH_2Cl_2 at room temperature are shown in Fig. 2. **YF1** displays a distinctly structured bluish-green emission spectrum centered at 486 nm with a shoulder at 518 nm due to a vibronic progression of ~1270 cm^{-1}. **YF2** possesses a less structured emission spectrum with a maximum emission peak at 500 nm and less discernible shoulder at ~535 nm also attributed to a vibronic progression (~1300 cm^{-1}). In both case the emission is attributed to a transition with mixed MLCT/LC character as previously reported[37] and as supported by theoretical calculations (see below). As shown in the inset of Fig. 3, the emission decay time of **YF1** and **YF2** were determined as 1.37 μs and 1.40 μs at room temperature, respectively. Compared to FIrpic (1.69 μs),[30] both novel iridium complexes show slightly shorter decay time. The photoluminescence quantum yields (Φ) of **YF1** and **YF2** are 0.52 and 0.61 in CH_2Cl_2. According to the decay time and luminescence yield, both the radiative and nonradiative rate constants (k_r and k_{nr}) were calculated to be ~10^5 s^{-1} (Table 2), in line with other bis-cyclometalated iridium complexes.[37] Compared to emission in solution, emissions with small bathochromic shift (ca. 10 ± 3 nm) were observed in neat films.

Electrochemical properties

The electrochemical properties of iridium complexes were recorded in solution in

CH$_2$Cl$_2$ by cyclic voltammetry (ESI†). Both iridium complexes show quasi-reversible oxidation waves at 0.77 and 0.60 V *vs*. Fc/Fc$^+$ for **YF1** and **YF2**, respectively, while the reduction waves could not be detected from 0 to –2.2 V (*vs* Fc/Fc$^+$). Therefore, the energy gaps were estimated from the edge of emission to be 2.7 eV and 2.6 for **YF1** and **YF2**, respectively. The HOMO and optical LUMO of **YF1** (–5.5/–2.8 eV) and **YF2** (–5.3/–2.7 eV) were evaluated via the empirical formula of $E_{HOMO} = -(1.2 \times E_{ox} + 4.6)$ eV and $E_{LUMO} = (E_{HOMO} + E_{00})$ eV.[38] The picolinate ancillary ligand stabilizes the HOMO while the optical LUMOs have very similar energy pointing to a similar photoactive LUMO for the two complexes as supported by theoretical calculations (see below).
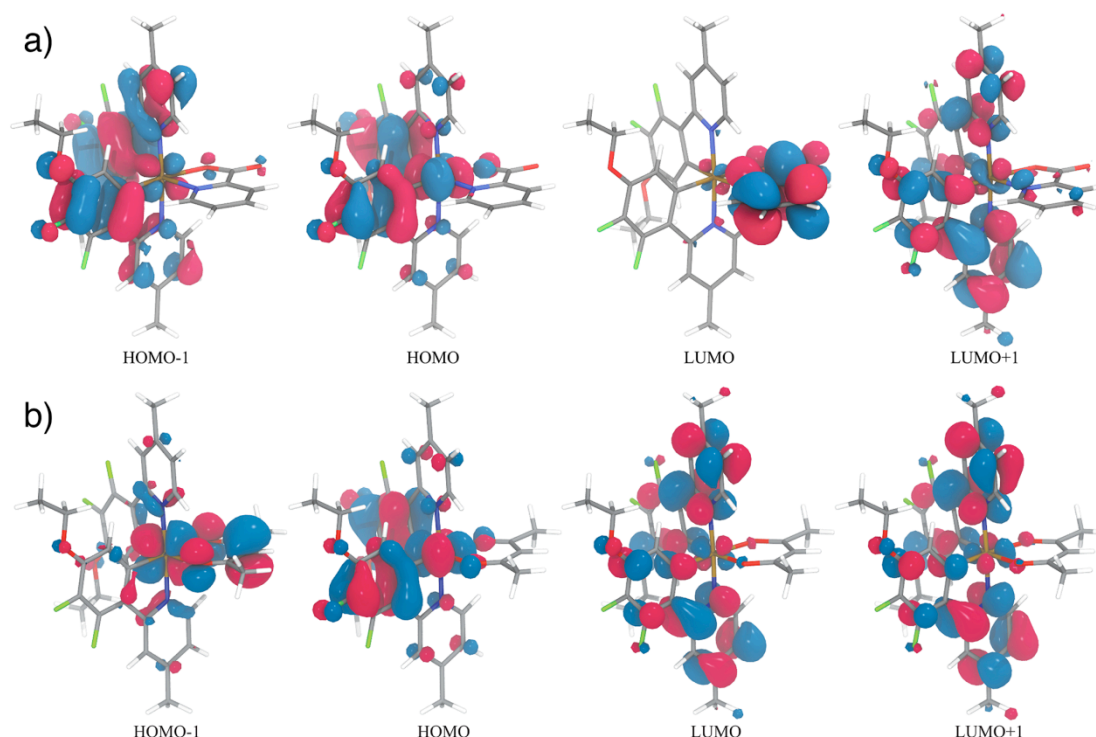

Fig. 3 Kohn-Sham molecular orbitals around the HOMO-LUMO gap for the ground-state optimized geometry obtained at the DFT/PBE0/TZVP(LANL2DZ)/IEFPCM(CH$_2$Cl$_2$) level of theory. Isovalue set to 0.03. a) **YF1** and b) **YF2**.

Theoretical characterization

The electronic structure of **YF1** and **YF2** were investigated by means of Density Functional Theory (DFT)[39, 40] and Linear-Response Time-Dependent Density Functional Theory (LR-TDDFT) using the PBE0[41, 42] exchange and correlation

functional (see ESI for a complete description of the computational protocol and additional information).[43-45] The Ir-C, Ir-N, and Ir-O bond lengths computed at the ground-state optimized geometries in gas phase are in close agreement with the X-ray diffraction data (Table 1). In particular, DFT/PBE0 accurately reproduces the slightly longer Ir-C bond length for the ppy ligand *trans* to the picolinate nitrogen.

Fig. 3 gives a representation of the Kohn-Sham (KS) molecular orbitals computed for the ground-state optimized geometry including implicit solvent effects (see computational details). As expected for cyclometalated iridium complexes, the HOMO of both complexes contains a contribution from the Ir(5d) orbital and extends on the phenyl part of the ppy ligands *via* a π-type orbital, with a small contribution from the fluorine atom in *para* position with respect to the carbanion. On the other hand, the LUMO is centered on the ancillary ligand for the **YF1** complex, whereas it is delocalized over both ppy ligands for the **YF2** molecule (a similar orbital corresponds to LUMO+1 and LUMO+2 for **YF1**). The adiabatic ionization energy of **YF1** (5.50 eV) is slightly higher than the one of **YF2** (5.36 eV), in good correlation with the experimental E_{HOMO}.
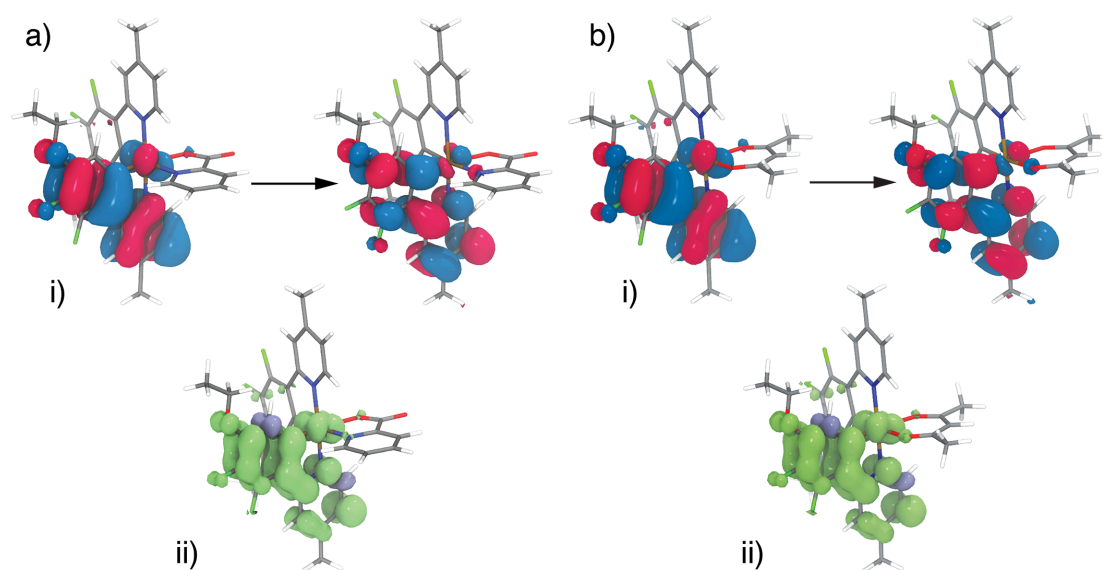

Fig. 4 Electronic character at the T_1 optimized geometry for a) **YF1** and b) **YF2**. i) NTOs representing the GS → T_1 at the LR-TDDFT/PBE0/TZVP(LANL2DZ)/IEFPCM(CH$_2$Cl$_2$) level of theory. ii) Contour plot of the spin density at the T_1 UDFT/PBE0/TZVP(LANL2DZ)/IEFPCM(CH$_2$Cl$_2$) optimized geometry.

UDFT and LR-TDDFT geometry optimizations were performed to shed some lights on the character of the emissive triplet state. Geometry optimization of the first triplet state at the LR-TDDFT/PBE0/TZVP(LANL2DZ)/IEFPCM(CH_2Cl_2) level of theory leads for both complexes to a molecular geometry, at which a triplet-to-singlet transition exhibits a MLCT/LC character. The natural transition orbitals (NTOs) characterizing the GS $\rightarrow$ T_1 transition at this particular triplet geometry are represented in Fig. 4ai) for **YF1** and 4bi) for **YF2**. It shows that the transition is localized on only one of the ppy ligand. To confirm the LR-TDDFT results, we further optimized the geometry with UDFT/PBE0. The spin density for the T_1 state at this new geometry (Fig. 4aii) for **YF1** and Fig. 4bii) for **YF2**) indicates a similar character than what was observed with LR-TDDFT.

The experimental maxima of emission are measured at rather similar energies, with 2.57 eV for **YF1** and 2.48 eV for **YF2**. Computing the adiabatic energy difference between the minimum at the T_1 UDFT/PBE0 optimized geometry and the minimum at the GS DFT/PBE0 optimized geometry also gives close values between the two complexes, with an energy of 2.63 eV for **YF1** (2.53 eV including zero-point energy) and 2.59 eV for **YF2** (2.49 eV including zero-point energy), hence reproducing the experimental trends.
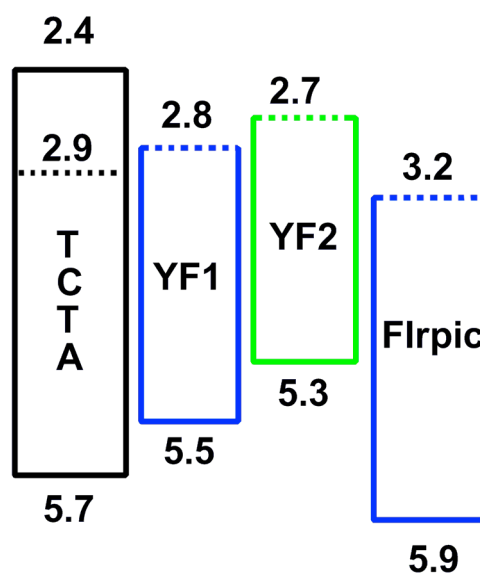

Fig. 5 Frontier energy levels of TCTA, **YF1**, **YF2** and **FIrpic**. Dashed lines denotes optical LUMO obtained as $E_{LUMO} = E_{HOMO} + E_{00}$.

13

Electroluminescence properties

To investigate the electroluminescent (EL) properties, **YF1** and **YF2** have been employed as the emitting dopants in solution-processed OLED with the configuration ITO/MoO$_3$ (8 nm)/N,N'-Bis-(1-naphthalenyl)-N,N'-bis-phenyl-(1,1'-biphenyl)-4,4'-diamine (NPB; 50 nm)/TCTA (5 nm)/TCTA: 8 wt% **YF1** or **YF2** (10 nm)/2,2′,2"-(1,3,5-Benzinetriyl)-tris(1-phenyl-1-H-benzimidazole) (TPBi; 30 nm)/LiF (1 nm)/Al. For comparison, FIrpic was also used as the phosphorescent dopant to fabricate OLEDs with a same device structure. The frontier energy levels of the host and the emitters are shown in Fig. 5.
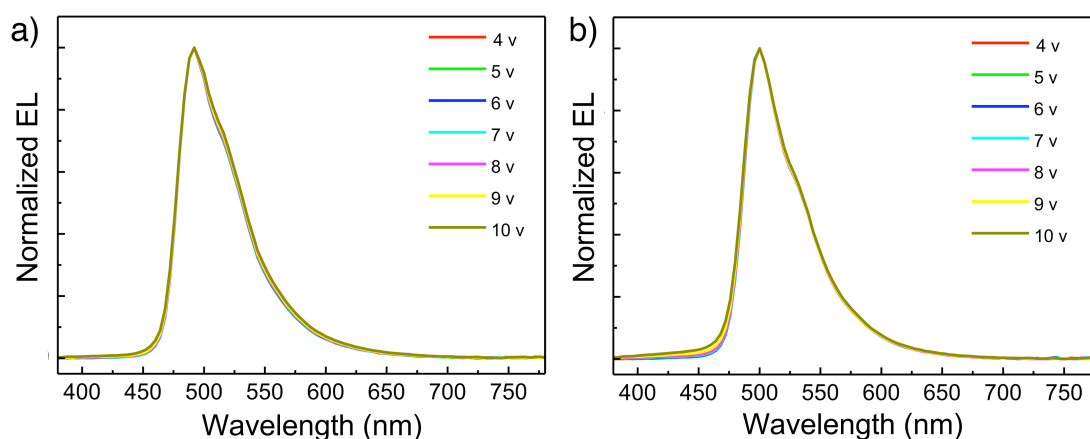

Fig. 6 Normalized EL spectra of a) device I (**YF1**) and b) device II (**YF2**) at voltages from 4V to 10 V

The electroluminescence (EL) spectra of devices doped with **YF1** (device I) and **YF2** (device 2) at different applied voltages are shown in Fig. 6. Devices I show stable bluish-green emission with a maximum emission peak at 492 nm from 4 V to 10 V. The Commission International de L'Éclairage (CIE) color coordinates of device I change only slightly from (0.18, 0.52) to (0.19, 0.51) in the range of applied voltages (ESI†). Device II present an emission with the maximum peak at 500 nm from 4 V to 10 V. As with device I, the CIE color coordinates of device II vary only slightly from (0.26, 0.57) to (0.28, 0.55) in the range of applied voltages (ESI†). This variation of CIE coordinates is due to the small rise of the high energy onset of the

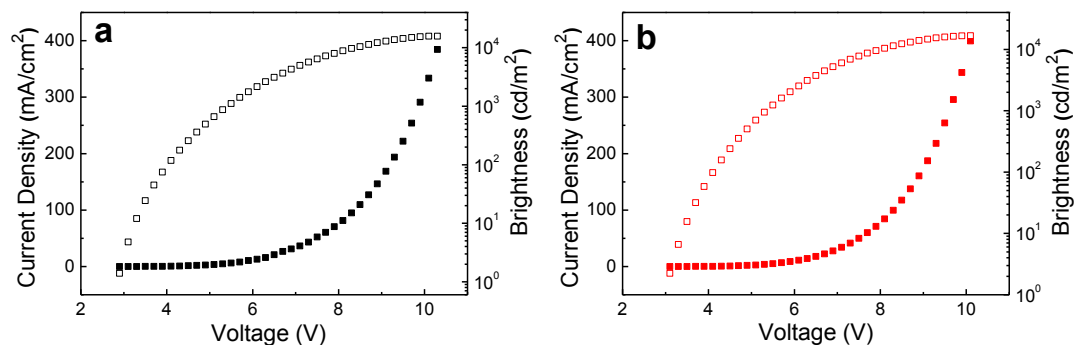electroluminescence spectra at ~450 nm as the voltage increases, which is attributed to emission from the host.[46]

Fig. 7 Current density-voltage-brightness (*J-V-L*) characteristics for device I (a, □: brightness, ■: current density) and device II (b, □: brightness, ■: current density)

The current density-voltage-brightness (*J-V-L*) characteristics of device I and II are shown in Fig. 7, and the corresponding data are summarized in Table 3. Device I has a very low turn on voltage of 2.8 V with a maximum luminance of 15,762 cd m^{-2} at 10 V (384 mA cm^{-2}). Device II gives a turn on voltage of 3.0 V with a maximum luminance of 16,727 cd m^{-2} at 10 V (400 mA cm^{-2}). Current efficiency of 19.6 cd A^{-1} and 26.0 cd A^{-1} were achieved for **YF1** and **YF2** devices at 100 cd m^{-2}, respectively (Fig. 8). Interestingly, these devices show a very small efficiency roll-off at practical brightness levels of 1000 cd m^{-2} and above. The current efficiencies retain 18.5 cd A^{-1} for device I and 25.1 cd A^{-1} for device II up to 1,000 cd m^{-2}. The efficiencies still held 16 cd A^{-1} and 22 cd A^{-1} at 3000 cd m^{-2}. Even at 5,000 cd m^{-2}, the efficiencies of both devices drop less than 30%. In addition, stable power efficiency of ~15 lm W^{-1} and ~20 lm W^{-1} (between 100 cd m^{-2} to 1,000 cd m^{-2}) are obtained for device I and device II, respectively, in sharp contrast with FIrpic-based device (Fig. S8, S9, and S12, ESI†). These results demonstrate that both of iridium complexes achieve stable performance in devices under a practical luminance level. Compared to the performance of FIrpic-based device (ESI†), device I and device II exhibit higher efficiencies and more stable device performances. From the comparison of frontier

energy levels of **YF1**, **YF2** and FIrpic with TCTA, the better performance of **YF1** and **YF2** are attributed to the better energetic match of these two complexes with the host matrix compared to FIrpic resulting in lower turn-on voltages.

Table 3. Performance of Devices I-III and FIrpic-based devcies

Devices	$V_{\text{turn-on}}$[a]	CE[b]	PE[b]	EQE[b]	Current efficiency roll-off (%)		
	V	cd A^{-1}	lm W^{-1}	%	1,000 cd m^{-2}	3,000 cd m^{-2}	5,000 cd m^{-2}
I	2.8	19.6	15.4	7.1	18.5 (5.6)	16 (18.4)	13.7 (30.1)
II	3	26.0	19.7	8.5	25.1 (3.5)	22 (15.4)	19.1 (26.5)
III	2.8	20.4	16.3	7.3	20.2 (1)	18 (11.7)	16.8 (17.6)
FIrpic	3.6	9.23	5.34	4.4	9.0 (2.6)	7.89 (14.5)	6.9 (25.2)

[a] the voltage is recorded at about 1 cd m^{-2}; [b] CE: current efficiency, PE: power efficiency, EQE: external quantum efficiency; The CE, PE and EQE are collected at 100 cd m^{-2}.
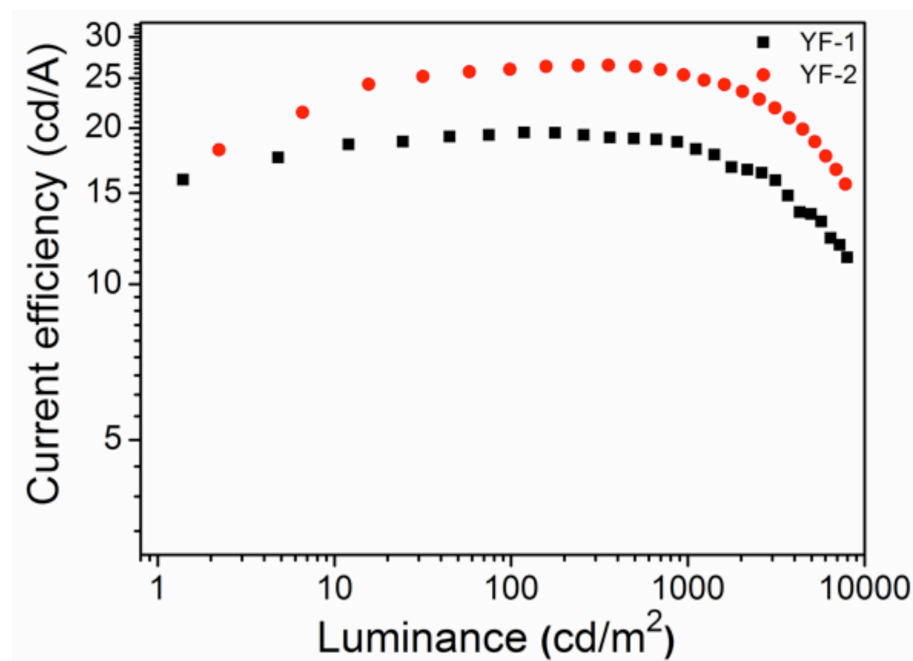

Fig. 8 Plots of current efficiency versus luminance for device I (■) and device II (■)
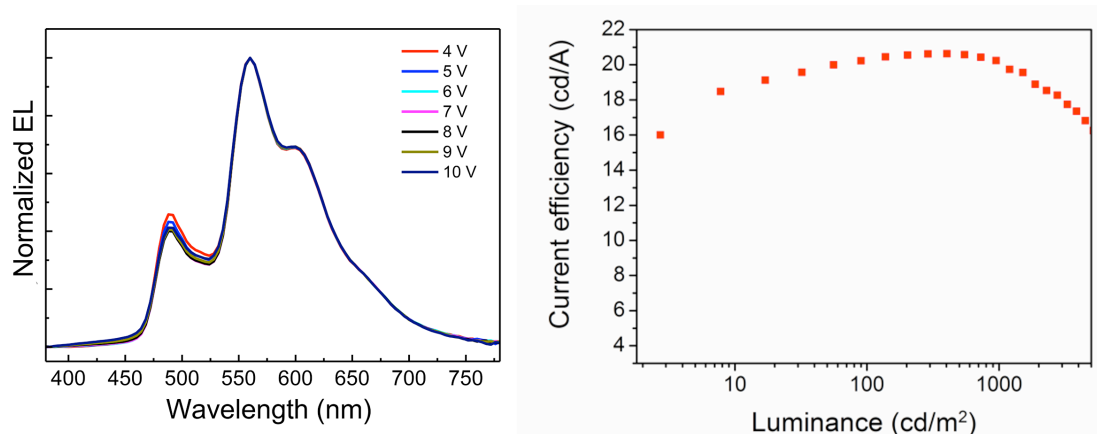
16

Fig. 9 EL spectra of device III at different voltages and plot of current efficiency *vs.* luminance

Because of the excellent color stability and attractive electroluminescence exhibited by **YF1**-based devices, next we prepared white OLEDs using **YF1** as bluish-green emitter and $Ir(bt)_2(acac)$ as orange emitter with the configuration ITO/MoO_3 (8 nm)/NPB (50 nm)/TCTA (5 nm)/TCTA: 6% $Ir(bt)_2(acac)$ (6 nm)/TCTA: 8% **YF1** (3 nm)/TPBi (30 nm)/LiF(1 nm)/Al. In Fig. 9, the device (device III) shows a broad emission covering the visible wavelength in a range from 450 to 750 nm. The emission band located at 489 nm is assigned to emission from **YF1** while the emission at long wavelength (560 nm, 603 nm) is attributed to $Ir(bt)_2(acac)$.[47, 48] The energy levels of the dopants match well with that of the host leading to quasi-no emission from the hosting matrix between 420-450 nm. The corresponding CIE coordinates of devices III are stable in the range of voltages used from (0.43, 0.49) to (0.43, 0.48) and belongs to the near-white emission region (Table S3, ESI†).

The curves of *J-V-L* for device III, as shown in Fig. 9, demonstrate a maximum brightness of 20,226 cd m^{-2} achieved at 11 V. This device exhibits a highest current efficiency of 20.4 cd A^{-1} and power efficiency of 16.3 lm W^{-1} at 100 cd m^{-2}. Interestingly, very small current efficiencies roll-off of less than 1% (20.2 cd A^{-1}) at 1,000 cd m^{-2} and less than 20% (16.8 cd A^{-1}) even at 5,000 cd m^{-2} were observed (Table 3 and Fig. 9).

Conclusion

In summary, two novel iridium complexes, **YF1** and **YF2**, have been synthesized and characterized. Both complexes display intense bluish-green emission. Because of the introduction of electron-donating ethyloxy group, there is a good match of the energy levels between the host and the emitters. As a result the turn-on voltage of electroluminescent devices is lowered (2.8-3.0 V) compared to the same device using FIrpic as the emitter (3.6 V). Improved external quantum efficiencies (EQE, η_{ext} = 7.5 and 8.1% at 100 cd m^{-2}) with attractively stable power efficiencies up to 1,000 cd m^{-2} compared to FIrpic (η_{ext} = 4.4% at 100 cd m^{-2}) are obtained while keeping reasonable efficiency roll-off $\leq$ 30% at luminance 5,000 cd m^{-2} and high color stability.

Color stable white OLEDs based on **YF1** show luminance of 20226 cd m^{-2} at 11 V and current efficiency of 20.4 cd A^{-1} at 100 cd m^{-2}. Interestingly, very small efficiency roll-off of about 1% at 1,000 cd m^{-2} and high color stability was achieved. At luminance level of 5,000 cd m^{-2} the roll-off efficiency is still below 20%.

This work demonstrates that the introduction of electron-donating substituents on a 2-phenylpyridine scaffold to obtain blue emitters with low oxidation potentials provides an alternative to strategies based on replacing the pyridine with imidazole, carbene, and pyrazole. This is advantageous as the latter strategies lead to materials with reduced chemical stability towards oxygen and/or increased lifetime of excited state. It is expected than, when combined with optimization of the device architecture (not done here), highly color-stable devices with low efficiency roll-off at high luminance will be obtained both for blue and white light electroluminescence.

Acknowledgement

References

1. M. A. Baldo, D. F. O'Brien, Y. You, A. Shoustikov, S. Sibley, M. E. Thompson and S. R. Forrest, *Nature*, 1998, **395**, 151.
2. C. Adachi, M. A. Baldo, M. E. Thompson and S. R. Forrest, *J. Appl. Phys.*, 2001, **90**, 5048.
3. S. Mukherjee and P. Thilagar, *Dyes and Pigments*, 2014, **110**, 2.
4. S. R. Forrest, *Org. Electron.*, 2003, **4**, 45.
5. N. Aizawa, Y. J. Pu, M. Watanabe, T. Chiba, K. Ideta, N. Toyota, M. Igarashi, Y. Suzuri, H. Sasabe and J. Kido, *Nat. Commun.*, 2014, **5**.
6. T. Chiba, Y. J. Pu, R. Miyazaki, K. Nakayama, H. Sasabe and J. Kido, *Org. Electron.*, 2011, **12**, 710.
7. J. Wang, F. J. Zhang, J. Zhang, W. H. Tang, A. W. Tang, H. S. Peng, Z. Xu, F. Teng and Y. S. Wang, *J. Photochem. Photobiol C*, 2013, **17**, 69.
8. S. Lamansky, P. Djurovich, D. Murphy, F. Abdel-Razzaq, H. E. Lee, C. Adachi, P. E. Burrows, S. R. Forrest and M. E. Thompson, *J. Am. Chem. Soc.*, 2001, **123**, 4304.
9. T. Tsuzuki and S. Tokito, *Adv. Mater.*, 2007, **19**, 276.
10. S. Lamansky, P. I. Djurovich, F. Abdel-Razzaq, S. Garon, D. L. Murphy and M. E. Thompson, *J. Appl. Phys.*, 2002, **92**, 1570.
11. V. V. Grushin, N. Herron, D. D. LeCloux, W. J. Marshall, V. A. Petrov and Y. Wang, *Chem. Commun.*, 2001, 1494.
12. C. Adachi, R. C. Kwong, P. Djurovich, V. Adamovich, M. A. Baldo, M. E. Thompson and S. R. Forrest, *Appl. Phys. Lett.*, 2001, **79**, 2082.
13. E. Baranoff and B. F. E. Curchod, *Dalton Trans.*, 2015, **44**, 8318.
14. S. Lee, S. O. Kim, H. Shin, H. J. Yun, K. Yang, S. K. Kwon, J. J. Kim and Y. H. Kim, *J. Am. Chem. Soc.*, 2013, **135**, 14321.
15. M. Marin-Suarez, B. F. E. Curchod, I. Tavernelli, U. Rothlisberger, R. Scopelliti, I. Jung, D. Di Censo, M. Gratzel, J. F. Fernandez-Sanchez, A. Fernandez-Gutierrez, M. K. Nazeeruddin and E. Baranoff, *Chem. Mater.*, 2012, **24**, 2330.
16. V. N. Kozhevnikov, K. Dahms and M. R. Bryce, *J. Org. Chem.*, 2011, **76**, 5143.
17. S. J. Lee, K. M. Park, K. Yang and Y. Kang, *Inorg. Chem.*, 2009, **48**, 1030.
18. R. J. Holmes, B. W. D'Andrade, S. R. Forrest, X. Ren, J. Li and M. E. Thompson, *Appl. Phys. Lett.*, 2003, **83**, 3818.
19. S. J. Su, H. Sasabe, T. Takeda and J. Kido, *Chem. Mater.*, 2008, **20**, 1691.
20. K. Udagawa, H. Sasabe, C. Cai and J. Kido, *Adv. Mater.*, 2014, **26**, 5062.
21. J. Y. Zhuang, W. F. Li, W. C. Wu, M. S. Song, W. M. Su, M. Zhou and Z. Cui, *New J. Chem.*, 2015, **39**, 246.
22. R. J. Holmes, S. R. Forrest, T. Sajoto, A. Tamayo, P. I. Djurovich, M. E. Thompson, J. Brooks, Y. J. Tung, B. W. D'Andrade, M. S. Weaver, R. C. Kwong and J. J. Brown, *Appl. Phys. Lett.*, 2005, **87**, 243507.
23. H. Sasabe, J.-I. Takamatsu, T. Motoyama, S. Watanabe, G. Wagenblast, N. Langer, O. Molt, E. Fuchs, C. Lennartz and J. Kido, *Adv. Mater.*, 2010, **22**, 5003.
24. C. H. Yang, S. W. Li, Y. Chi, Y. M. Cheng, Y. S. Yeh, P. T. Chou, G. H. Lee, C. H. Wang and C. F. Shu, *Inorg. Chem.*, 2005, **44**, 7770.

25. T. Sajoto, P. I. Djurovich, A. Tamayo, M. Yousufuddin, R. Bau, M. E. Thompson, R. J. Holmes and S. R. Forrest, *Inorg. Chem.*, 2005, **44**, 7992.

26. Z. Z. Li, Y. L. Niu, H. Y. Zhou, H. Y. Chao and B. H. Ye, *Inorg. Chem.*, 2013, **52**, 10087.

27. E. Baranoff, S. Fantacci, F. De Angelis, X. Zhang, R. Scopelliti, M. Grätzel and M. K. Nazeeruddin, *Inorg. Chem.*, 2011, **50**, 451.

28. T. Sajoto, P. I. Djurovich, A. B. Tamayo, J. Oxgaard, W. A. Goddard and M. E. Thompson, *J. Am. Chem. Soc.*, 2009, **131**, 9813.

29. J. Frey, B. F. E. Curchod, R. Scopelliti, I. Tavernelli, U. Rothlisberger, M. K. Nazeeruddin and E. Baranoff, *Dalton Trans.*, 2014, **43**, 5667.

30. E. Baranoff, B. F. E. Curchod, F. Monti, F. Steimer, G. Accorsi, I. Tavernelli, U. Rothlisberger, R. Scopelliti, M. Grätzel and M. K. Nazeeruddin, *Inorg. Chem.*, 2012, **51**, 799.

31. J. N. Demas and G. A. Crosby, *J. Phys. Chem.*, 1971, **75**, 991.

32. N. Sun, Q. Wang, Y. B. Zhao, Y. H. Chen, D. Z. Yang, F. C. Zhao, J. S. Chen and D. G. Ma, *Adv. Mater.*, 2014, **26**, 1617.

33. S. Sprouse, K. A. King, P. J. Spellane and R. J. Watts, *J. Am. Chem. Soc.*, 1984, **106**, 6647.

34. S. Lamansky, P. Djurovich, D. Murphy, F. Abdel-Razzaq, R. Kwong, I. Tsyba, M. Bortz, B. Mui, R. Bau and M. E. Thompson, *Inorg. Chem.*, 2001, **40**, 1704.

35. B. Schmid, F. O. Garces and R. J. Watts, *Inorg. Chem.*, 1994, **33**, 9.

36. A. Tsuboyama, H. Iwawaki, M. Furugori, T. Mukaide, J. Kamatani, S. Igawa, T. Moriyama, S. Miura, T. Takiguchi, S. Okada, M. Hoshino and K. Ueno, *J. Am. Chem. Soc.*, 2003, **125**, 12971.

37. J. Li, P. I. Djurovich, B. D. Alleyne, M. Yousufuddin, N. N. Ho, J. C. Thomas, J. C. Peters, R. Bau and M. E. Thompson, *Inorg. Chem.*, 2005, **44**, 1713.

38. B. W. D'andrade, S. Datta, S. R. Forrest, P. Djurovich, E. Polikarpov and M. E. Thompson, *Org. Electron.*, 2005, **6**, 11.

39. P. Hohenberg and W. Kohn, *Phys Rev B*, 1964, **136**, B864.

40. W. Kohn and L. J. Sham, *Phys Rev*, 1965, **140**, 1133.

41. J. P. Perdew, M. Ernzerhof and K. Burke, *J. Chem. Phys.*, 1996, **105**, 9982.

42. C. Adamo and V. Barone, *J. Chem. Phys.*, 1999, **110**, 6158.

43. M. E. Casida, in *Recent Advances in Density Functional Methods*, ed. D. P. Chong, World Scientific, Singapore, 1995, p. 155.

44. E. Runge and E. K. U. Gross, *Phys. Rev. Lett.*, 1984, **52**, 997.

45. M. Petersilka, U. J. Gossmann and E. K. U. Gross, *Phys. Rev. Lett.*, 1996, **76**, 1212.

46. N. Sun, Q. Wang, Y. B. Zhao, D. Z. Yang, F. C. Zhao, J. S. Chen and D. G. Ma, *J. Mater. Chem. C*, 2014, **2**, 7494.

47. L. P. Zhu, Y. B. Zhao, H. M. Zhang, J. S. Chen and D. G. Ma, *J. Appl. Phys.*, 2014, **115**.

48. W. J. Finkenzeller, T. Hofbeck, M. E. Thompson and H. Yersin, *Inorg. Chem.*, 2007, **46**, 5076.